Research

Alterations in gap junction connexin43/connexin45 ratio mediate a transition from quiescence to excitation in a mathematical model of the myometrium

Rachel E. Sheldon[1,3], Chipo Mashayamombe[2,3], Shao-Qing Shi[4], Robert E. Garfield[4], Anatoly Shmygol[3], Andrew M. Blanks[3] and Hugo A. van den Berg[1]

[1]MOAC Doctoral Training Centre, and [2]Systems Biology Doctoral Training Centre, University of Warwick, Coventry CV4 7AL, UK
[3]Division of Reproductive Health, Warwick Medical School, Coventry CV2 2DX, UK
[4]Department of Obstetrics and Gynecology, St Joseph's Hospital and Medical Center, Phoenix 85013, AZ, USA

The smooth muscle cells of the uterus contract in unison during delivery. These cells achieve coordinated activity via electrical connections called gap junctions which consist of aggregated connexin proteins such as connexin43 and connexin45. The density of gap junctions governs the excitability of the myometrium (among other factors). An increase in gap junction density occurs immediately prior to parturition. We extend a mathematical model of the myometrium by incorporating the voltage-dependence of gap junctions that has been demonstrated in the experimental literature. Two functional subtypes exist, corresponding to systems with predominantly connexin43 and predominantly connexin45, respectively. Our simulation results indicate that the gap junction protein connexin45 acts as a negative modulator of uterine excitability, and hence, activity. A network with a higher proportion of connexin45 relative to connexin43 is unable to excite every cell. Connexin45 has much more rapid gating kinetics than connexin43 which we show limits the maximum duration of a local burst of activity. We propose that this effect regulates the degree of synchronous excitation attained during a contraction. Our results support the hypothesis that as labour approaches, connexin45 is downregulated to allow action potentials to spread more readily through the myometrium.

1. Introduction

The myometrium, which makes up the bulk of the uterine wall in all species [1] (electronic supplementary material, figures S1*a* and S1*b*), is composed of interconnected smooth muscle cells, which form an excitable medium [2], i.e. a medium that is capable of propagating signals over relatively long distances with virtually no damping. In the myometrium, these propagating signals take the form of action potentials which trigger phasic contractions during labour [3]. These involve the rhythmic contraction and relaxation of the smooth muscle cells, giving rise to synchronized travelling waves throughout the uterus [4]. In humans, the phasic contractions typically last for around a minute [5], whereas in rats, they last for approximately 68 s at term [6].

Throughout most of pregnancy, the myometrium remains quiescent, allowing the fetus to develop undisturbed [7]. The myometrium undergoes major changes in the days leading up to labour [7]. In particular, as parturition approaches, the uterus becomes more excitable through an activation phase which involves molecular changes that lead to a decrease in time between subsequent contractions [8]. In humans, this interval decreases from
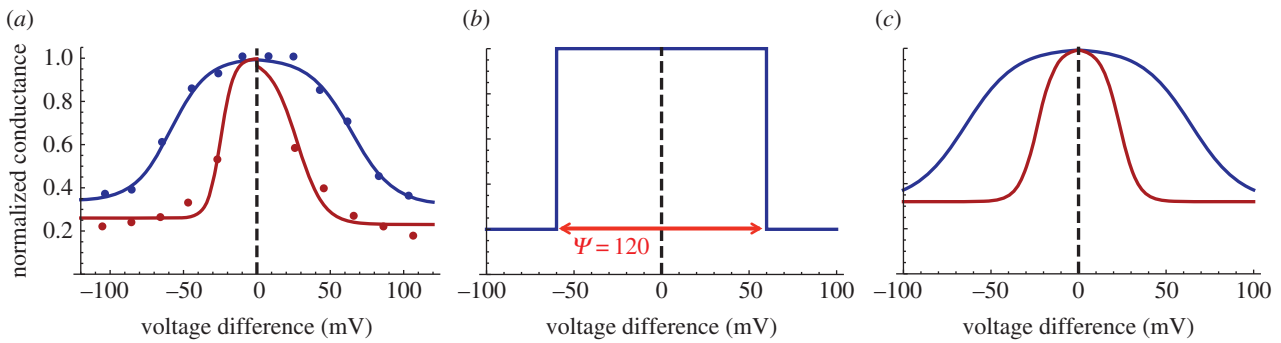
Figure 1. (a) Relationship between conductance and voltage difference between neighbouring cells as published by Miyoshi et al. [25]. The blue line shows the type I gap junction relationship identified; the red line shows the type II gap junction relationship identified. Points show experimental conductances determined by Miyoshi et al. [25]. The lines represent Boltzmann curve fits to the data (equation (2.3)); (b) step function describing the relationship between voltage difference and gap-junctional conductance. A value $\psi = 120$ corresponds to a conductance of 1 over a voltage difference of ± 60 mV and (c) symmetrical curves for the type I relationship (blue) and the type II relationship (red) identified by Miyoshi et al. [25]. Type II is determined from type I by a change in the parameter ψ in equation (2.4). (Online version in colour.)

approximately 30 min to approximately 2 min as labour progresses [5,8], whereas in rats, contractions occur at 2.3 min intervals at gestational day 19 and at 46 s intervals in active labour [6].

A key condition for the transition to excitability at the whole-organ level is a change in connectivity between the myometrial smooth muscle cells [2]. The smooth muscle cells in the myometrium are connected through a series of intercellular channels that allow the passage of ions and small molecules from one cell to another, each channel being made up of two components, one contributed by each cell [9].

As pregnancy progresses, the density of gap junctions on the cell-to-cell contact surfaces increases, which is thought to be one of many factors that instigate labour [2]. In the non-pregnant uterus of both rats and humans, gap junctions are either absent or present at low density [2,10,11]. At the time of delivery, gap junctions are present at a density of approximately 1000 per cell in human tissue [12].

The ability of a myometrial network to achieve global excitation is strongly dependent on spatial heterogeneity of cell-to-cell connectivity [13]. Using a mathematical model of the myometrium based on FitzHugh–Nagumo dynamics [14,15], we previously showed that a moderate degree of spatial heterogeneity allows excitation to spread throughout a network even if the same network would be quiescent when fully and uniformly connected. However, the coupling between cells was represented as a passive resistor, whereas, in reality, voltage-dependent gating is a well-established property of vertebrate gap junction channels [16–19]. This transjunctional voltage-dependence is directly related to the connexin composition of the channel. Individual connexins exhibit different responses as a function of the potential difference between neighbouring cells; for example, connexin43 (Cx43) is relatively insensitive to the voltage difference, displaying only modest changes in conductance as the transjunctional voltage is altered [20]. By contrast, connexin45 (Cx45) and connexin40 are highly sensitive to transjunctional voltage differences [20–22]. The differences in connexin protein response to transjunctional voltage are thought to be underpinned by different localizations of charged residues along the inner lining of the ion-conducting pore as well as different phosphorylation states [23,24].

Miyoshi et al. [25] recorded gap-junctional currents between isolated pairs of rat myometrial cells, using the double-whole-cell voltage-clamp configuration (electronic supplementary material, figure S3). The cell pairs were found to exhibit one of two distinct relationships between

conductance and voltage-dependence which occurred in equal proportions (figure 1a). The so-called type I channels displayed a gradual increase from a normalized conductance of 0.2–1 with decreasing voltage difference. At small transjunctional voltages, there was very little change in conductance. By contrast, the 'type II' channels showed a much sharper increase in conductance with decreasing voltage difference. A notable voltage-dependent change in conductance was observed even at small transjunctional voltages. The authors observed that the type I voltage-dependence relationship fitted with the pattern expected for a tissue with predominantly Cx43 junction proteins. In addition, the type II junction voltage-dependence appeared to be notably distinct from the connexin patterns observed before. The dependence of conductance on the transjunctional voltage difference for type II is more consistent with a Cx45 junction protein, a hypothesis that was further supported by the findings by Moreno et al. [26].

Here, we investigate how the spread of excitation through a network is affected by incorporating voltage-dependent cell-to-cell couplings in the mathematical model. We adapt the voltage-dependent conductance relationships for both gap junction types identified by Miyoshi et al. [25]. The main qualitative effect is that conductance increases as the potential difference between the cells decreases. To isolate this 'cut-off' effect, we initially model the voltage-dependence relationship as a simple step function. We subsequently compare our findings with more realistic voltage-conductance relationships in order to verify that the dominant qualitative effect is the 'cut-off' point of activity.

Finally, we incorporate gating kinetics. We propose that the type II gap junctions are not able to excite the network by themselves; a substantial proportion of type I gap junctions is needed to spread activity effectively. The gating kinetics is much more rapid for type II gap junctions in comparison with type I junctions. The faster kinetics prevents the longer depolarization propagating throughout the network, and so limits the excitability of the network. Accordingly, we suggest that relative proportions of type I and type II gap junctions are crucial for the modulation of activity in the excitable myometrial network.

Analysis of gene expression in rat models suggests that the expression of Cx45 is downregulated in labour. We do not observe a change in the expression of Cx43 in the transition from pregnancy to labour. We therefore hypothesize that the relative proportion of Cx43 and Cx45 is crucial; Cx45 acts as

Table 1. Parameter values used in equations (2.1a) and (2.1b) in all simulations.

parameter	B	α	γ	w_0	V_0	ϵ
value	3	3	0.05	0.4	0.4	0.2

a brake on activity in the uterus, and its downregulation may be an important step in the initiation of labour.

2. Methods

2.1. Mathematical modelling

We further develop a mathematical model of the myometrial smooth muscle network [13]. The network is constructed as a square lattice in which each node is connected to four others. Each simulated cell obeys FitzHugh–Nagumo dynamics. The FitzHugh–Nagumo model is a two-variable system that describes the excitation and relaxation of an excitable cell [27]. The model is an example of an excitation–relaxation oscillator owing to its threshold properties in which a sufficiently large input of current is required for the cell to exhibit an excursion corresponding to excitation and relaxation. However, parameters can be chosen such that cells are autorhythmic [13], that is, the cells continually oscillate through the excitation–relaxation cycle without any external stimulus. FitzHugh–Nagumo is a simplification of the Hodgkin–Huxley model for spiking neurons [28,29] and, as such, is often used in modelling excitable systems such as contractions of cardiac myocytes [30–32].

Each node in the network is considered to be an excitation–relaxation oscillator with a fast ('excitation') state variable v that corresponds to the transmembrane potential and a slow ('recovery') variable w that corresponds to gating kinetics which repolarize the excited cell. The following dimensionless ordinary differential equations describe this two-variable model

$$\frac{\mathrm{d}}{\mathrm{d}t}v(t) = \frac{1}{\epsilon}(Bv(t)(1-v(t))(v(t)-\alpha)-w(t)-w_0)+I \quad (2.1a)$$

and

$$\frac{\mathrm{d}}{\mathrm{d}t}w(t) = v(t)-\gamma w(t)-v_0, \quad (2.1b)$$

where I is the input current and B, α, γ, w_0, v_0, and ϵ are positive parameters. The values shown in table 1 are used in all simulations to generate a network of cells which require a suprathreshold current input to undergo an oscillation.

The equations were solved using a Livermore solver for ordinary differential equations approach through the NDSolve function in MATHEMATICA. Results were numerically stable under variation in step size.

Each simulated cell is coupled to its four neighbours through resistors representing gap junctions (electronic supplementary material, figure S2a). A coupling constant K is assigned to each gap junction and defined as $K_{ij} = (C_i R_{ij})^{-1}$, where i and j are two neighbouring cells, C_i is the capacitance of cell i, and R_{ij} is the resistance between the two cells. The coupling K is therefore a rate constant, and is rendered dimensionless as follows. The FitzHugh–Nagumo model defines dimensionless time, t, as $t = R_1/\tau D$, where D is a damping coefficient that captures the inertia of the system owing to the gating kinetics, as shown by FitzHugh [14], τ is dimensional time and R_1 is the passive resistance of the nonlinear current device, represented as a tunnel diode by Nagumo et al. [15]. Accordingly, dimensionless coupling is defined as D/R_1K and denoted by κ. The scaling of the remaining parameters is detailed in the appendix and follows the derivation given by Keener & Sneyd [27].

Miyoshi et al. [25] identified two distinct relationships between the conductance of smooth muscle gap junctions and the voltage difference between two neighbouring myocytes (figure 1a). We adapt these relationships to represent voltage-dependent gap junctions in terms of the coupling strength κ. Spatial heterogeneity is added to the system by introducing a probability p of a connection existing between any two adjacent cells, as previously described [13]. This parameter is referred to as the 'connectivity' of the network. The relative cluster size serves as a measure of the proportion of cells in the network that become excited: if all cells are excited, the relative cluster size equals 1, whereas, if no cells become excited, it is 0.

2.1.1. Step function model

The simplest way to represent the voltage-dependence is by means of a step function (figure 1b). For cells with a small voltage difference, the normalized gap-junctional conductance is set to be 1, whereas for cells with a large voltage difference, the normalized gap-junctional conductance is 0.2 (the base value determined by Miyoshi et al. [25]). We use the term *gap-junctional conductance bandwidth* to mean the range of voltage differences for which the gap-junctional conductance equals 1. The voltage differences are scaled from unit-bearing values to the dimensionless FitzHugh–Nagumo model values. To facilitate numerical analysis, the step function is smoothed, as follows (electronic supplementary material, figure S4a,b)

$$\text{relative conductance} = 0.6$$
$$+ \frac{0.4 \times (\psi/2 - |((v_i(t)-v_j(t)) \times \lambda)|)}{\sqrt{1 + (\psi/2 - |((v_i(t)-v_j(t)) \times \lambda)|)^2}}, \quad (2.2)$$

where the indices i and j represent adjacent cells, λ is the scaling required to convert between physiological values and the FitzHugh–Nagumo model values, and ψ is the gap-junctional conductance bandwidth. The relative conductance is multiplied by the coupling strength κ. In the majority of simulations, $\kappa = 1$; however, we also present some results with $\kappa = 0.76$ to facilitate comparison with previous results in which we demonstrated the importance of heterogeneity [13].

Scaling is based on a typical rat myometrial cell in accordance with Miyoshi et al. [25]. The membrane potential of a rat myometrial cell increases from -45 to $+10$ mV during the upstroke of a full action potential, corresponding to an excursion of 55 mV. In the non-dimensionalized model, the size of the excursion is 3.52278. Accordingly, λ is taken to be 55/3.52278. To vary the width of the gap-junctional conductance band ψ is selected from the range 40 to 200 mV (twice the difference to zero, which lies at the midpoint). The value of ψ then dictates the voltage difference values over which the conductance of the gap junction equals 1. For example, $\psi = 120$ mV sets the conductance to 1 over a voltage difference of ± 60 mV, as illustrated in figure 1b.

To check the model against our previous findings, the bandwidth is set to a sufficiently high value such that the relative conductance remains 1 over the entire voltage range of the action potential. The proportion of cells that become excited as a function of connectivity p reproduce our previous results; see the electronic supplementary material, figure S5 for more details. With a coupling strength $\kappa = 0.76$, we replicate our previous scenarios in which spatial heterogeneity proved to be crucial in exciting the network (electronic supplementary material, figure S6).

2.1.2. Symmetrical Miyoshi model

Miyoshi et al. [25] proposed the following empirical equation for the conductance–voltage relationship

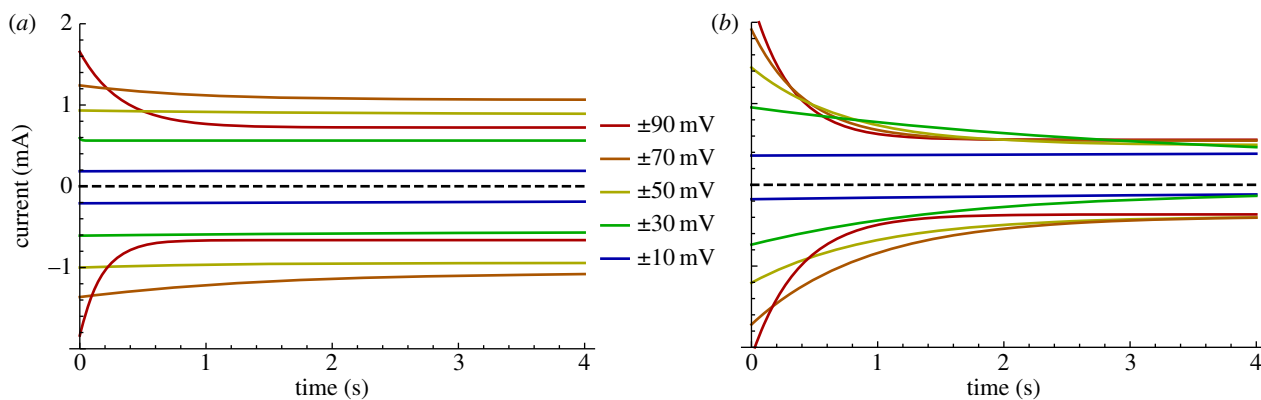$$g(V_j) = \frac{(1-G_{\min})}{1+\exp\{-A(V_j-V_h)\}}+G_{\min}, \quad (2.3)$$

Figure 2. Gap junction current responses over time following step pulses of voltages between ± 90 mV. Pulses of ± 90 mV are shown in red, ± 70 mV in orange, ± 50 mV in yellow, ± 30 mV in green and ± 10 mV in blue. Lines shown are curve fits to experimental data published by Miyoshi et al. [17]. (a) The type I response and (b) the type II response. (Online version in colour.)

Table 2. Parameter values for equation (2.3).

	negative V_j			positive V_j		
	G_{min}^-	V_h^- (mV)	A^- (mV^{-1})	G_{min}^+	V_h^+ (mV)	A^+ (mV^{-1})
type I	0.34	-58.5	0.08	0.32	64.4	-0.07
type II	0.26	-24.6	0.23	0.23	27.3	-0.11

where g is the normalized conductance of the gap junction, V_j is the voltage difference across the gap junction, G_{min} is the minimum value of the conductance, V_h is the half inactivation voltage (mV) at which the conductance is reduced by $(1 - G_{min})/2$, and A is a slope factor ((mV)$^{-1}$). The authors identified two distinct types of voltage-dependent gap junctions with the parameters given in table 2. The relationship between the voltage gradient and gap-junctional conductance is shown for both types in figure 1a.

To investigate the effect of the width of the gap-junctional conductance band, we model the type I relationship by means of the bandwidth parameter ψ that allows us to scale the type I relationship to resemble the type II relationship. We employ a symmetrical version by taking the absolute value of the voltage and using the positive values that Miyoshi et al. [25] obtained for the Boltzmann fit, as shown in the equation (2.4)

$$g(V_j) = \frac{(1 - G_{min}^+)}{1 + \exp\{-A^+(|V_j \times \lambda \times 110/\psi| - V_h^+)\}} + G_{min}^+, \quad (2.4)$$

where λ is the scaling required to convert between physiological values and FitzHugh–Nagumo values, and ψ is the required width of the gap-junctional conductance band. For instance, $\psi = 110$ mV will give type I, and $\psi = 40$ mV will give type II. The scaling parameter $\lambda = 55/3.52278$, as before. A pictorial representation of the symmetrical Miyoshi model [25] is shown in figure 1c.

We checked the model against our previous results by setting the bandwidth to a high value in order to attain a relative conductance of 1 over the action potential voltage range (electronic supplementary material, figure S7).

2.1.3. Symmetrical Miyoshi model with gating kinetics
The dependence of conductance on trans-gap-junctional voltage as described in §2.1.2 is non-dynamic, i.e. the gating kinetics is sufficiently rapid to justify a quasi-instantaneous model. We now turn to more realistic gating kinetics. In the first instance,

voltage-dependence of the time constant is ignored, giving rise to the following ordinary differential equation

$$\frac{\mathrm{d}}{\mathrm{d}t}g = \frac{1}{\tau_g}(\bar{g}(V_j) - g), \quad (2.5)$$

where g is the conductance of an individual gap junction, τ_g is the gap-junctional time constant, and $\bar{g}$ is the steady-state conductance dependent on the transjunctional voltage V_j as considered in §§2.1.1 and 2.1.2. A complete excitation–relaxation cycle in the FitzHugh–Nagumo model lasts for 18.6849 dimensionless units (the time at which the cell is able to become re-excited) and we assume an action potential burst in the rat lasts for around 30 s. Therefore, to convert from dimensionless time to seconds, we multiply the dimensionless time by 30/18.6849.

We next consider a model in which the time constant τ_g is dependent on the potential difference between neighbouring cells. The voltage-dependence relationship for the time constants is derived from Miyoshi et al. [25] by considering the gap-junctional current response after 5 s step pulses of voltages in the range ± 90 mV (figure 2a,b, respectively). The type I and type II gap junctions exhibit distinct relationships, given in figure 2. An exponential equation is fitted using the least-squares criterion to each current response in order to determine the time constant for each voltage difference. A Gaussian is then fitted using the least-squares criterion to the time constants giving voltage-dependent time constant relationships as follows:

$$\text{time constant} = a \times e^{-(V_j^2/2b^2)} + c, \quad (2.6)$$

where V_j is the transjunctional voltage, $a = 9.39726$, $b = 23.9757$, and $c = 0.60274$ for type I, and $a = 9.41999$, $b = 16.799$, and $c = 0.580013$ for type II (figure 3). We are not able to obtain good estimates of the rate of decay near 0 mV, because the time constant here substantially exceeds the duration of the experiment.

2.2. Experimental methods
We employed rat models in order to investigate the changes in expression of Cx43 and Cx45 in the myometrium between gestational
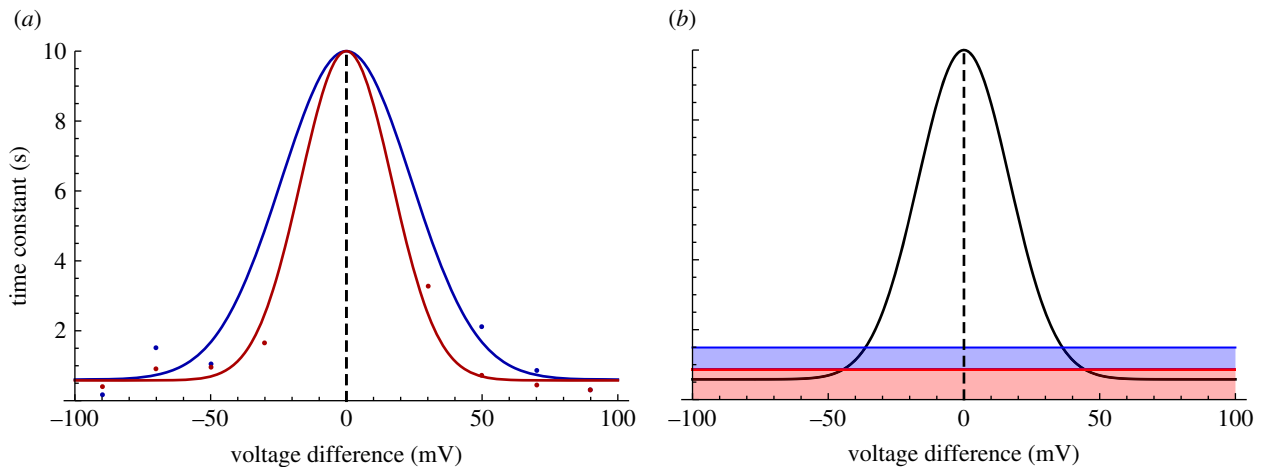
Figure 3. (*a*) The relationships between voltage difference between neighbouring cells and the time constant of the gap junctions. The type I relationship is shown in red, and the type II relationship is shown in blue; (*b*) comparison of voltage difference between neighbouring cells and the time constant of the gap junction for type II junctions (as in figure 3). The red-shaded region indicates time constants for the type II junctions in which no excitation is possible. The blue-shaded region indicates time constants for the type II junctions in which spatial heterogeneity is necessary for excitation to take place. (Online version in colour.)
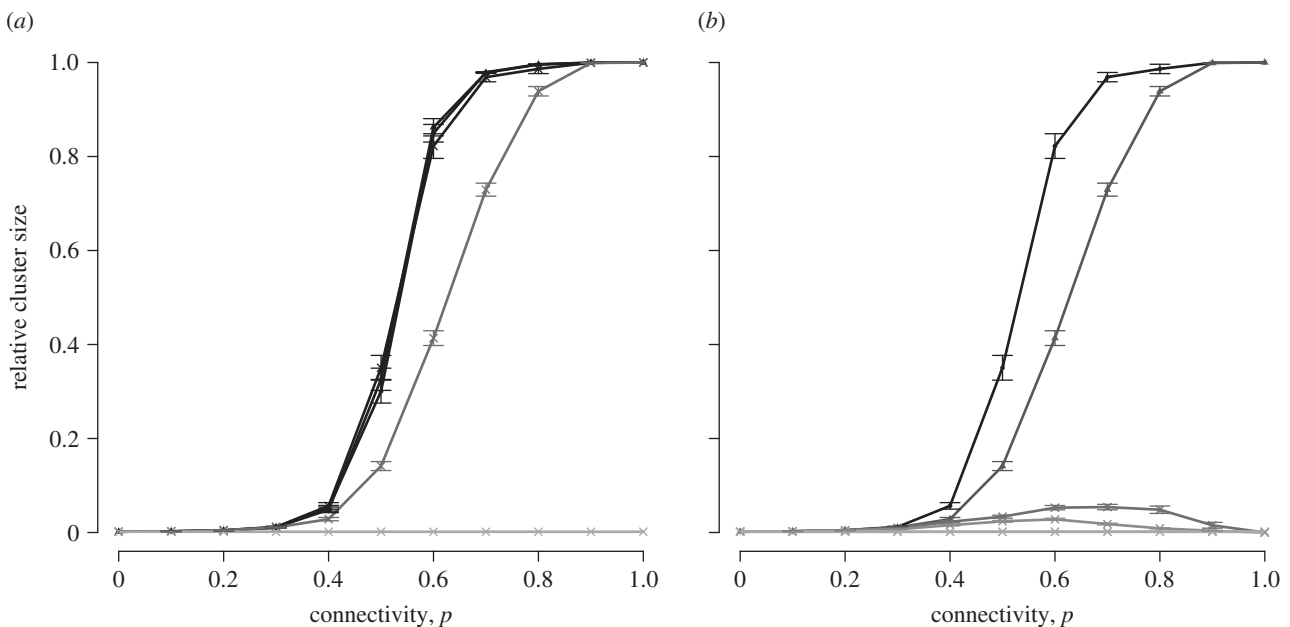

Figure 4. Relative cluster size versus connectivity p for a lattice with gap-junctional conductance related to voltage-dependence with a step function. Points show mean $\pm$ s.e.m. of 100 simulations for a 25×25 lattice. In all simulations, an initial perturbation of 1 was used. Lines represent the different widths of the gap-junctional conductance band in the step function model. (*a*) Widths of 100, 80, and 60 mV are shown in black, and widths of 40 and 20 mV are shown on a graded scale from dark to light; (*b*) lines show widths of 60, 40, 39, 38, 30, and 20 mV on a graded scale from dark to light. Activity is lost between widths of 40 and 39 mV.

ages of 19.25 and 22 days. Detailed experimental methods are provided in the electronic supplementary material, §S1.1.

3. Results

The effect of varying the gap-junctional conductance bandwidth is studied first. We then examine cases in which the conductance relaxes to a steady state over a certain period of time. In more sophisticated simulations, the time constant is dependent on the voltage difference between neighbouring cells.

3.1. Minimal gap-junctional conductance bandwidth

Numerical simulations with the step function model indicate that there is a critical minimal gap-junctional conductance band below which global excitation cannot be achieved (figure 4*a*). For conductance bandwidths of 100, 80, 60, and

40 mV, full activity is observed with a fully connected lattice. However, once the conductance bandwidth drops lower than 40 mV, all activity disappears, and only the perturbed cell is capable of being excited. The transition from excitation to quiescence is quite steep and takes place over a very small range of bandwidth values: between 40 and 39 mV (figure 4*b*). Simulations with several lattice sizes indicate that this transition has the character of a discontinuous phase transition in the limit of infinite lattice size (see electronic supplementary material, figures S8 and S9 for further details).

The critical value of the bandwidth is located between the apparent bandwidth values of type I and type II gap junctions as described by Miyoshi *et al.* [25] (figure 5*a*). This strongly suggests that physiological significance can be attached to the qualitative difference between bandwidths for which no global excitation is achieved, and those bandwidths that permit global excitation.
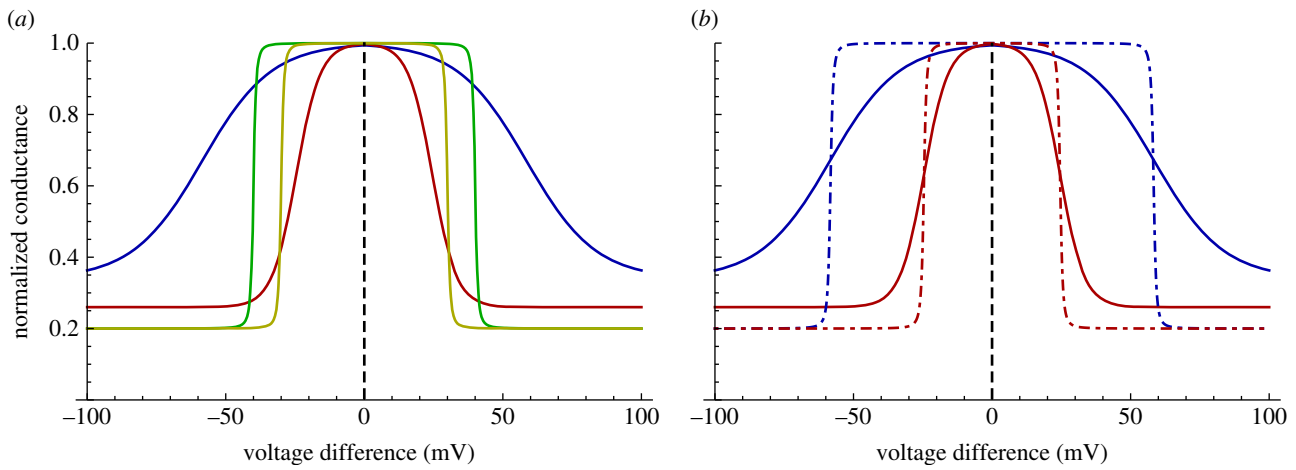
Figure 5. The relationship between conductance and voltage difference for a selection of models. The solid blue and solid red lines represent the Miyoshi et al. [25] type I and II models, respectively. (a) The green and yellow lines represent step function widths at the extremes of the critical range of values for total loss of excitability; (b) the blue and red dot-dashed lines represent widths outside the critical range, chosen to coincide with the midpoints of conductances of the type I and type II models, respectively. (Online version in colour.)
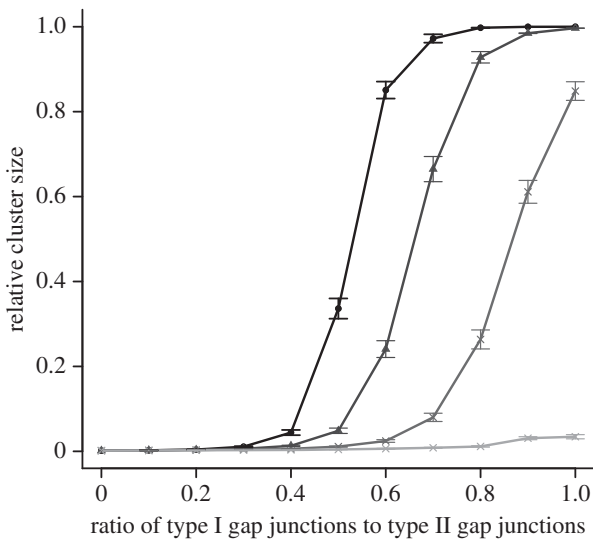

Figure 6. The relationship between the proportion of cells that become excited, and the ratio of type I gap junctions (i.e. excitation possible) to type II gap junctions (i.e. excitation impossible), for a smoothed step function model. Lines show probabilities of connections existing between any two cells of 1, 0.8, 0.6, and 0.4 on a graded scale from dark to light. Points show mean $\pm$ s.e.m. of 100 simulations for a 25×25 lattice, all with an initial perturbation of 1.

To assess the hypothesis that the threshold bandwidth value is significant, we ran simulations in which cell-to-cell couplings were randomly assigned the bandwidth corresponding to type I or type II, using probabilities of intercell connections of 0.4, 0.6, 0.8, and 1. The relative cluster size increases with the proportion of type I gap junctions (figure 6), with a steep increase between ratios of type II to type I gap junctions of 0.4 and 0.6. This qualitative result is also found with lower connection probabilities. As the connectivity of the lattice is decreased, the transition values shift in favour of a larger proportion of type I gap junctions.

The qualitative results obtained with the step function model were repeated in a model which more closely represented the shape of the type I and type II [25] fits (see §2.1.2). There is a minimum gap-junctional conductance bandwidth beyond

which no excitation can take place, and a clear transition between excited and quiescent states. The results of this simulation are detailed in electronic supplementary material, figures S10 and S11.

Network activity depends on the connectivity p and the ratio of type II to type I gap junctions. Figure 7 suggests that there is a defined set of conditions that promote network excitation. The majority of parameter combinations result in no activity. However, a network with high connectivity and a higher proportion of type I gap junctions relative to type II gap junctions maximizes the likelihood of near full activity.

3.2. The effect of gating kinetics

Here, we examine the symmetrical Miyoshi model with voltage-gated gap junctions using a fixed time constant. The excitability of a network with exclusively type I gap junctions is unaffected by the value of the time constant—there is always full activity at full connectivity (figure 8a). By contrast, the time constant is a key parameter in a network with type II gap junctions. With a small time constant, type II gap junctions are unable to propagate any activity, as before. However, as the time constant is increased, the relationship between connectivity and relative cluster size assumes one of two distinct forms (figure 8b). For time constants between 0.87 and 1.49 s (0.54 and 0.93 in dimensionless units), the relationship follows a bell-shaped curve, indicative of the importance of spatial heterogeneity in exciting the network. For time constants larger than 1.51 s (0.94 in dimensionless units), the relationship follows a sigmoidal curve in which full connectivity corresponds to full excitation. These results are summarized in table 3.

Comparisons are drawn between the time constant thresholds identified above, and the time constant relationship with voltage difference for type II gap junctions (figure 3b). For a voltage difference greater than ± 50 mV, excitation in the network is not possible. For voltage differences less than ± 35 mV, excitation is always possible. When the voltage difference is between ± 35 and ± 50 mV, spatial heterogeneity in connections is essential to obtain excitation in the network.

Finally, we examine a network with varying proportions of type I and type II gap junctions. As before, cell-to-cell couplings were randomly assigned the bandwidth corresponding
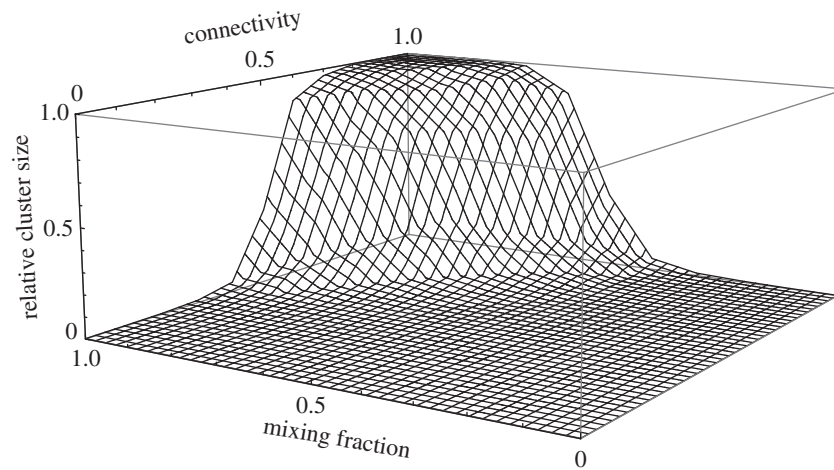
Figure 7. Three-dimensional illustration of the network activity (relative cluster size) with varying connectivity p and proportion of type I and type II gap junctions. Each point in the mesh represents the mean of 100 simulations for a 25×25 lattice with an initial perturbation of 1. The density of the grid indicates that a larger proportion of cells is able to become excited with higher connectivity, and a greater proportion of type I gap junctions than type II gap junctions.
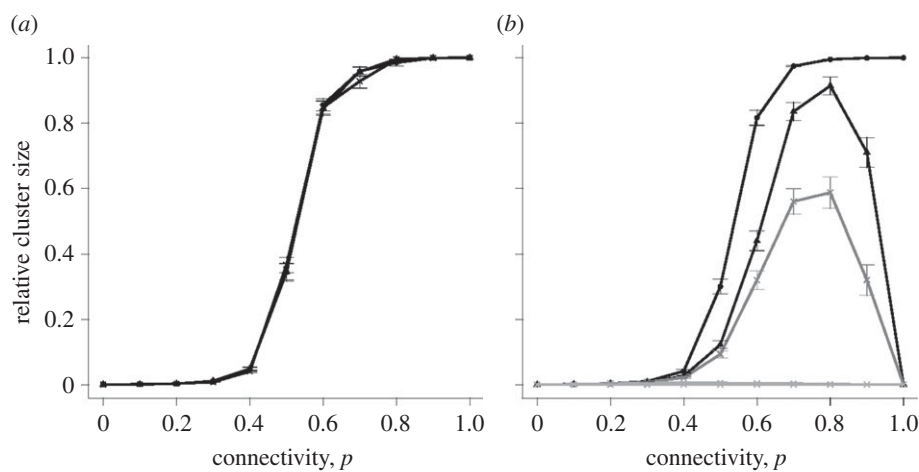

Figure 8. Relative cluster size versus connectivity p for a dynamic coupled lattice which relaxes back to the steady state in a fixed time period represented by different lines. Points show mean $\pm$ s.e.m. of 100 simulations for a 25×25 lattice. In all simulations, an initial perturbation of 1 was used. The lines represent different time constant values. (*a*) Type I gap junctions. Lines represent time constants of 1, 0.5, and 0.1 s all shown in black owing to their close proximity; (*b*) type II gap junctions. Lines represent time constants of 1, 0.9, 0.7, 0.5, and 0.1 s on a graded scale from dark to light.

Table 3. Summary of the excitation threshold time constants for type II gap junctions.

time constant (model units)	time constant (s)	result
$t \geq 1$	$\tau \geq 1.162$	sigmoidal shape
$0.1 \leq t \leq 0.9$	$0.116 \leq \tau \leq 1.046$	bell shape
$t < 0.1$	$\tau < 0.116$	no activity

to type I or type II. In addition, the voltage-dependent time constants corresponding to the chosen bandwidth are incorporated into the model using the Gaussian fit detailed in equation (2.6). Type II gap junctions remain unable to produce full network excitation even at full connectivity (figure 9). A small influence of spatial heterogeneity is apparent for networks with exclusively type II gap junctions. Around 20% of cells are able to become excited with connectivities in the range 0.6–0.8. Type I gap junctions are unaffected by the switch to voltage-dependent time constants. The cells in

the network are still able to exhibit full activity with full connectivity. As the connectivity is reduced, so is the excitation.

3.3. Experimental results
Transcriptomics data suggest that expression of connexin45 (Cx45) in the inner myometrium is substantially lower on gestation day 22 (in labour) when compared with gestation day 19.25 (figure 10*a*). On the other hand, there does not appear to be a difference in connexin43 (Cx43) expression between these two points in time in either the inner or outer myometrium (figure 10*b*). Taken together, these data would suggest an increase of the Cx43 : Cx45 ratio, i.e. a relative enrichment of Cx43.

4. Discussion
Our findings suggest that the relative proportions of connexin43 (Cx43) and connexin45 (Cx45) are vital in initiating contractions in the myometrium during parturition. We build on the results obtained by Miyoshi *et al*. [25] to show that global excitation can be attained in a model network
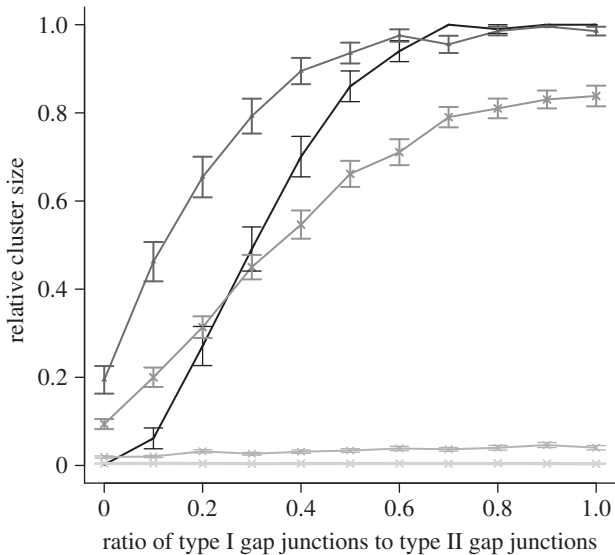
Figure 9. The relationship between the proportion of cells that become excited, and the ratio of type I gap junctions to type II gap junctions, for a model with dynamic gap-junctional conductances. Lines show probabilities of connections existing between any two cells of 1, 0.8, 0.6, 0.4, and 0.2 on a graded scale from dark to light. Points show mean $\pm$ s.e.m. of 100 simulations for a 25 $\times$ 25 lattice, with an initial perturbation of 1.

Figure 10. Gene expression of (a) connexin45 (Cx45) in the inner and outer myometrium; (b) connexin43 (Cx43) in the inner and outer myometrium at rat gestation days 19.25 and 22 (in labour, LAB). Lines show the mean gene expression $\pm$ s.d. with $n = 3$ for gestation day 19.25 and $n = 2$ for gestation day 22 (LAB).

relying solely on Cx43 proteins, whereas this is not the case for a system using only Cx45. In addition, we develop a model in which the conductance of a gap junction is dynamic and has a voltage-dependent time constant, Cx45 having faster gating kinetics than Cx43. We demonstrated that this time constant is a key factor in determining whether global excitation can be achieved. At shorter time constants, heterogeneity in the density of gap junction connections plays a more prominent role in deciding whether activity can spread.

In rodents (as in most mammals, but not humans [33]), the myometrium can be divided into two distinct layers of smooth muscle: the inner circular layer and the outer longitudinal layer [34]. Our experimental data indicate downregulation of Cx45 expression in the rat as labour approaches, in contrast to Cx43 expression where no change at the end of pregnancy appears to be evident. Chan et al. [35] found similar results in human myometrium, analysing the RNA of myometrial samples from pregnant women (five from women in labour, and five from women at full term, but not in labour). These authors showed that Cx43 expression remains unchanged between the two sample groups, whereas Cx45 expression is significantly downregulated in the 'in labour' group in comparison with the 'not-in-labour' group (electronic supplementary material, figure S12). These results are in accordance with our data, which furthermore suggest that the significant changes found by Chan et al. [35] were owing to changes in expression taking place in the inner myometrium as opposed to the outer myometrium. Our model simulations show that an elevated proportion of Cx43 proteins is a key factor in modulating conductance. This accords well with results obtained by Döring et al. [36] and Tong et al. [37], who found that in a Cx43 knockout mouse, the lack of intracellular myometrial coupling results in weaker contractions and delayed labour. These various lines of evidence strongly suggest that the Cx43 : Cx45 ratio is instrumental in controlling the global excitability of the myometriocyte network.

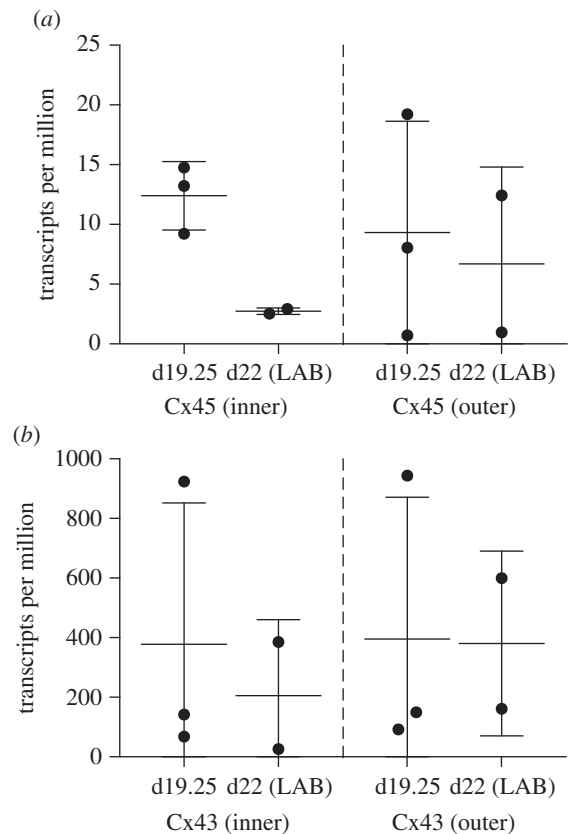The connexin protein Cx45 plays an important role in cardiac myocytes; it is found in the atrioventricular (AV) node

and the adjoining His bundles [38,39]. While Cx45 is not essential for continued survival in the adult mouse [39], Cx45 knockout mice die from heart failure in utero [40,41]. Without Cx45, contractions initiated in the AV node are not coordinated with the contractions in the ventricles; Cx45 may play a similar role in the myometrium, i.e. to inhibit contractions until the development of the fetus has advanced sufficiently for delivery. The inviability of Cx45 knockout mouse embryos [40,41] precludes a test of this hypothesis in vivo. However, Cx45 knockout in vitro studies could be used to demonstrate the development of global network events.

Voltage-dependent gap junctions have previously been considered in mathematical models [42,43]. Baigent et al. [44,45] and Donnell et al. [46] considered a two-cell model coupled by a dynamic gap junction which resides in one of three states, giving insights into cell connections on a local scale, emphasizing channel kinetics and ionic flows in great detail. By contrast, the present model focuses on overall excitability of the network as a function of spatial heterogeneity of the functional properties of the gap junctions, rather than on the propagation of activity wavefronts and the spatial patterning of such fronts; these aspects have been considered elsewhere [4,32,47,48]. Whereas we considered the global activation threshold in an electrotonically coupled smooth muscle syncytium, a general argument regarding the all-or-none character of synaptically coupled networks, such as the central nervous system, was advanced by Ashby et al. [49].

This work has not considered heteromeric gap-junction channels with both Cx45 and Cx43 proteins. We assumed that the relationships given by Miyoshi et al. [25] correspond

to homomeric gap junction channels. Martinez *et al.* [50] demonstrated that these two gap junction proteins are co-expressed in cardiac cells, and that homomeric channels of either Cx45 or Cx43 have different unitary conductances. A heteromeric gap-junction channel might exhibit non-symmetrical behaviour; this will require further experimental studies in order to inform our model.

We do not report an increase in Cx43 expression in the rat between day 19.25 and day 22. This finding is in keeping with the literature in that the rise in Cx43 occurs prior to parturition (4 days before term in the rat). Cx43 proteins are stored in vesicles and only trafficked to the membrane gap junctions when labour commences, so causing an increase in functional expression in labour, but not an increase in gene expression in the tissue [11,51–55]. Studies using immunohistochemistry and Western blot analysis have demonstrated the functional increase in Cx43 expression at term as well as a decrease in Cx45 [56,57]. Albrecht *et al.* [56] suggested that the ratio of Cx43 to Cx45 might be crucial for increased network connectivity associated with the initiation of labour, which is in agreement with our finding that relative numbers of Cx43 and Cx45 are a key permissive factor—Cx45 effectively acting as a brake on contractile activity in the uterus. As parturition approaches, Cx45 becomes downregulated, allowing contractions to increase in strength and frequency.

Appendix A. Derivation of the FitzHugh–Nagumo model

We follow the derivation provided by Keener & Sneyd [27]. Consider the circuit given in the electronic supplementary material, figure S2*b* showing a simplified model of the cell membrane. From Kirchoff's laws, one obtains

$$C_m \frac{\mathrm{d}V}{\mathrm{d}\tau} + F(V) + i = -I_0 \tag{A 1a}$$

and

$$D \frac{\mathrm{d}i}{\mathrm{d}\tau} + Ri = V - V_0, \tag{A 1b}$$

where I_0 is the applied external current, i is the current through the resistor–inductor, $V = V_i - V_e$ is the membrane potential, R is the resistance, and V_0 is the potential gain across the battery which forms part of the excitable element representing the recovery current in electronic supplementary material, figure S2*b*. D is the damping coefficient, which captures the inertia of the system induced by the gating kinetics, as shown by FitzHugh in 1961 [14]. R and D are incorporated into the 'excitable element'. Here, τ represents dimensional time. The function $F(V)$ is a cubic with three zeros: the smallest $V = 0$ and largest $V = V_1$ are stable solutions of $\mathrm{d}V/\mathrm{d}\tau = -F(V)$. The passive resistance of the nonlinear element (defined as a tunnel diode by Nagumo [15]) is $R_1 = 1/F'(0)$.

The equations are rendered dimensionless as follows. Define $v = V/V_1$, $w = R_1 i/V_1$, $f(v) = -R_1 F(V_1 v)/V_1$, and $t = R_1 \tau/L$. Equations (A 1) can then be rewritten as follows

$$\epsilon \frac{\mathrm{d}v}{\mathrm{d}t} = f(v) - w - w_0 \tag{A 2a}$$

and

$$\frac{\mathrm{d}w}{\mathrm{d}t} = v - \gamma w - v_0, \tag{A 2b}$$

where $\epsilon = R_1^2 C_m/D$, $w_0 = R_1 I_0/V_1$, $v_0 = V_0/V_1$, and $\gamma = R/R_1$. The function $f(v)$ is a cubic and can be written as follows

$$f(v) = Av(v - \alpha)(1 - v). \tag{A 3}$$

References

1. Putz R, Pabst R. 1989 *Sobotta: atlas of human anatomy*, 14th edn. Munich, Germany: Elsevier.

2. Garfield RE, Sims S, Daniel EE. 1977 Gap junctions: their presence and necessity in myometrium during parturition. *Science* **198**, 958–960. (doi:10.1126/science.929182)

3. Parkington HC, Tonta MA, Davies NK, Brennecke SP, Coleman HA. 1999 Hyperpolarization and slowing of the rate of contraction in human uterus in pregnancy by prostaglandins E₂ and F₂α: involvement of the Na⁺ pump. *J. Physiol.* **514**, 229–243. (doi:10.1111/j.1469-7793.1999.229af.x)

4. Singh R, Xu J, Garnier NG, Pumir A, Sinha S. 2012 Self-organized transition to coherent activity in disordered media. *Phys. Rev. Lett.* **108**, 068102. (doi:10.1103/PhysRevLett.108.068102)

5. Maeda K. 2013 Uterine contractions in normal labor developed by a positive feed-back and oscillation. *J. Health Med. Informat.* **4**, 130. (doi:10.4172/2157-7420.1000130)

6. Buhimschi C, Boyle MB, Saade GR, Garfield RE. 1998 Uterine activity during pregnancy and labor assessed by simultaneous recordings from the myometrium and abdominal surface in the rat. *Am. J. Obstet. Gynecol.* **178**, 811–822. (doi:10.1016/S0002-9378(98)70498-3)

7. Challis JRG, Matthews SG, Gibb W, Lye SJ. 2000 Endocrine and paracrine regulation of birth at term and preterm. *Endocr. Rev.* **21**, 514–550. (doi:10.1210/er.21.5.514)

8. Parkington HC, Tonta MA, Brennecke SP, Coleman HA. 1999 Contractile activity, membrane potential, and cytoplasmic calcium in human uterine smooth muscle in the third trimester of pregnancy and during labor. *Am. J. Obstet. Gynecol.* **181**, 1445–1451. (doi:10.1016/S0002-9378(99) 70390-X)

9. Kumar NM, Gilula NB. 1996 The gap junction communication channel. *Cell* **84**, 381–388. (doi:10.1016/S0092-8674(00)81282-9)

10. Garfield RE, Sims SM, Kannan MS, Daniel EE. 1978 Possible role of gap junctions in activation of myometrium during parturition. *Am. J. Physiol.* **235**, C168–C179.

11. Risek B, Guthrie S, Kumar N, Gilula NB. 1990 Modulation of gap junction transcript and protein expression during pregnancy in the rat. *J. Cell Biol.* **110**, 269–282. (doi:10.1083/jcb.110.2.269)

12. Garfield RE, Blennerhassett MG, Miller SM. 1988 Control of myometrial contractility: role and regulation of gap junctions. *Oxf. Rev. Reprod. Biol.* **10**, 436–490.

13. Sheldon RE, Baghdadi M, McCloskey C, Blanks AM, Shmygol A, van den Berg HA. 2013 Spatial heterogeneity enhances and modulates excitability in a mathematical model of the myometrium. *J. R. Soc. Interface* **10**, 20130458. (doi:10.1098/rsif.2013.0458)

14. FitzHugh R. 1961 Impulses and physiological states in theoretical models of nerve membrane. *Biophys. J.* **1**, 445–466. (doi:10.1016/S0006-3495(61)86902-6)

15. Nagumo J, Arimoto S, Yoshizawa S. 1962 An active pulse transmission line simulating nerve axon. *Proc. IRE* **50**, 2061–2070. (doi:10.1109/JRPROC.1962.288235)

16. Spray DC, Harris AL, Bennett MVL. 1979 Voltage-dependence of junctional conductance in early amphibian embryos. *Science* **204**, 432–434. (doi:10.1126/science.312530)

17. Spray DC, Harris AL, Bennett MVL. 1981 Equilibrium properties of a voltage-dependent junctional conductance. *J. Gen. Physiol.* **77**, 77–93. (doi:10.1085/jgp.77.1.77)

18. Harris AL, Spray DC, Bennett MVL. 1981 Kinetic properties of a voltage-dependent junctional conductance. *J. Gen. Physiol.* **77**, 95–117. (doi:10.1085/jgp.77.1.95)

19. Wang H-Z, Li J, Lemanski LF, Veenstra RD. 1992 Gating of mammalian cardiac gap junction channels by trans-junctional voltage. *Biophys. J.* **63**, 139–151. (doi:10.1016/S0006-3495(92)81573-4)

20. Veenstra RD, Wang H-Z, Westphale EM, Beyer EC. 1992 Multiple connexins confer distinct regulatory and conductance properties of gap junctions in developing heart. *Circ. Res.* **71**, 1277–1283. (doi:10.1161/01.RES.71.5.1277)

21. Veenstra RD, Wang H-Z, Beyer EC, Bring PR. 1994 Selective dye and ionic permeability of gap junction channels formed by connexin45. *Circ. Res.* **75**, 483–490. (doi:10.1161/01.RES.75.3.483)

22. Beblo DA, Wang H-Z, Beyer EC, Westphale EM, Veenstra RD. 1995 Unique conductance, gating, and selective permeability properties of gap junction channels formed by connexin40. *Circ. Res.* **77**, 813–822. (doi:10.1161/01.RES.77.4.813)

23. Verselis YK, Ginter CS, Bargiello TA. 1994 Opposite voltage gating polarities of two closely related connexins. *Nature* **368**, 348–351. (doi:10.1038/368348a0)

24. Moreno AP, Fishman GI, Spray DC. 1992 Phosphorylation shifts unitary conductance and modifies voltage-dependent kinetics of human connexin43 gap junction channels. *Biophsy. J.* **62**, 51–53. (doi:10.1016/S0006-3495(92)81775-7)

25. Miyoshi H, Boyle MB, MacKay LB, Garfield RE. 1996 Voltage-clamp studies of gap junctions between uterine muscle cells during term and preterm labor. *Biophys. J.* **71**, 1324–1334. (doi:10.1016/S0006-3495(96)79332-3)

26. Moreno AP, Laing JG, Beyer EC, Spray DC. 1995 Properties of gap junction channels formed of connexin 45 endogenously expressed in human hepatoma (SKHep1) cells. *Am. J. Physiol. Cell Physiol.* **268**, C356–C365.

27. Keener J, Sneyd J. 1998 Excitability. In *Mathematical physiology* (eds JE Marsden, L Sirovich, S Wiggins), pp. 116–159. New York, NY: Springer.

28. Hodgkin AL, Huxley AF, Katz B. 1952 Measurement of current–voltage relations in the membrane of the giant axon of *Loligo*. *J. Physiol.* **116**, 424–448.

29. Hodgkin AL, Huxley AF. 1952 A quantitative description of membrane current and its application to conduction and excitation in nerve. *J. Physiol.* **177**, 500–544.

30. Zhang H, Holden AV. 1995 Chaotic meander of spiral waves in the FitzHugh–Nagumo system. *Chaos, Solitons Fractals* **5**, 661–670. (doi:10.1016/0960-0779(93)E0048-G)

31. Aliev RR, Panfilov AV. 1996 A simple two-variable model of cardiac excitation. *Chaos, Solitons Fractals* **7**, 292–301. (doi:10.1016/0960-0779(95)00089-5)

32. Benson AP, Clayton RH, Holden AV, Kharche S, Tong WC. 2006 Endogenous driving and synchronization in cardiac and uterine virtual tissues: bifurcations and local coupling. *Phil. Trans. R. Soc. A* **364**, 1313–1327. (doi:10.1098/rsta.2006.1772)

33. Weiss S, Jaermann T, Schmid P, Staempfli P, Boesiger P, Niederer P, Caduff R, Bajka M. 2006 Three-dimensional fiber architecture of the nonpregnant human uterus determined *ex vivo* using magnetic resonance diffusion tensor imaging. *Anat. Rec. A Discov. Mol. Cell Evol. Biol.* **288**, 84–90. (doi:10.1002/ar.a.20274)

34. Brody JR, Cunha GR. 1989 Histologic, morphometric, and immunocytochemical analysis of myometrial development in rats and mice: II. Effects of DES on development. *Am. J. Anat.* **186**, 21–42. (doi:10.1002/aja.1001860103)

35. Chan Y-W, van den Berg HA, Moore JD, Quenby S, Blanks AM. 2014 Assessment of myometrial transcriptome changes associated with spontaneous human labour by high throughput RNA-seq. *Exp. Physiol.* **99**, 510–524. (doi:10.1113/expphysiol.2013.072868)

36. Döring B *et al.* 2006 Ablation of connexin43 in uterine smooth muscle cells of the mouse causes delayed parturition. *J. Cell Sci.* **119**, 1715–1722. (doi:10.1242/jcs.02892)

37. Tong D, Lu X, Wang H-W, Plante I, Lui E, Laird DW, Bai D, Kidder GM. 2009 A dominant loss-of-function GJA1 (Cx43) mutant impairs parturition in the mouse. *Biol. Reprod.* **80**, 1099–1106. (doi:10.1095/biolreprod.108.071969)

38. Gourdie RG, Lo CW. 1999 Cx43 (α1) gap junctions in cardiac development and disease. *Curr. Top. Membr.* **49**, 581–602. (doi:10.1016/S0070-2161(08)61030-8)

39. Frank M *et al.* 2012 Connexin45 provides optimal atrioventricular nodal conduction in the adult mouse heart. *Circ. Res.* **111**, 1528–1538. (doi:10.1161/CIRCRESAHA.112.270561)

40. Kumai M, Nishii K, Nakamura JI, Takeda N, Suzuki M, Shibata Y. 2000 Loss of connexin45 causes a cushion defect in early cardiogenesis. *Development* **127**, 3501–3512.

41. Krüger O *et al.* 2000 Defective vascular development in connexin 45-deficient mice. *Development* **127**, 4179–4193.

42. Vogel R, Weingart R. 1998 Mathematical model of vertebrate gap junctions derived from electrical measurements on homotypic and heterotypic channels. *J. Physiol.* **510**, 177–189. (doi:10.1111/j.1469-7793.1998.177bz.x)

43. Chen-Izu Y, Moreno AP, Spangler RA. 2001 Opposing gates model for voltage gating of gap junction channels. *Am. J. Physiol. Cell Physiol.* **281**, C1604–C1613.

44. Baigent S, Stark J, Warner A. 1997 Modelling the effect of gap junction nonlinearities in systems of coupled cells. *J. Theor. Biol.* **186**, 223–229. (doi:10.1006/jtbi.1996.0351)

45. Baignet S. 2003 Cells coupled by voltage-dependent gap junctions: the asymptotic dynamical limit. *Biosystems* **68**, 213–222. (doi:10.1016/S0303-2647(02)00097-7)

46. Donnell P, Baigent S, Banaji M. 2009 Monotone dynamics of two cells dynamically coupled by a voltage-dependent gap junction. *J. Theor. Biol.* **261**, 120–125. (doi:10.1016/j.jtbi.2009.07.012)

47. Barkley D. 1991 A model for fast computer simulation of waves in excitable media. *Physica D* **49**, 61–70. (doi:10.1016/0167-2789(91)90194-E)

48. Bub G, Shrier A, Glass L. 2002 Spiral wave generation in heterogeneous excitable media. *Phys. Rev. Lett.* **88**, 058101. (doi:10.1103/PhysRevLett.88.058101)

49. Ashby WR, von Foerster H, Walker CC. 1962 Instability of pulse activity in a net with threshold. *Nature* **196**, 561–562. (doi:10.1038/196561a0)

50. Martinez AD, Hayrapetyan V, Moreno AP, Beyer EC. 2002 Connexin43 and connexin45 form heteromeric gap junction channels in which individual components determine permeability and regulation. *Circ. Res.* **90**, 1100–1107. (doi:10.1161/01.RES.0000019580.64013.31)

51. Winterhager E, Stutenkemper R, Traub O, Beyer E, Willecke K. 1991 Expression of different connexin genes in rat uterus during decidualization and at term. *Eur. J. Cell Biol.* **55**, 133–142.

52. Hendrix EM, Mao SJT, Everson W, Larsen WJ. 1992 Myometrial connexin 43 trafficking and gap junction assembly at term and preterm labor. *Mol. Reprod. Dev.* **33**, 27–38. (doi:10.1002/mrd.1080330105)

53. Tabb T, Thilander G, Grover A, Hertzberg E, Garfield RE. 1992 An immunochemical and immunocytological study of the increase in myometrial gap junctions (and connexin 43) in rats and humans during pregnancy. *Am. J. Obstet. Gynecol.* **167**, 559–567. (doi:10.1016/S0002-9378(11)91453-7)

54. Garfield RE, Hayashi RH. 1981 Appearance of gap junctions in the myometrium of women during labor. *Am. J. Obstet. Gynecol.* **140**, 958–959.

55. Nielsen MS, Axelsen LN, Sorgen PL, Verma V, Delmar M, Holstein-Rathlou NH. 2012 Gap junctions. *Compr. Physiol.* **2**, 1981–2035. (doi:10.1002/cphy.c110051)

56. Albrecht JL, Atal NS, Tadros PN, Orsino A, Lye SJ, Sadovsky Y, Beyer E. 1996 Rat uterine myometrium contains the gap junction protein connexin45, which has a differing temporal expression pattern from connexin43. *Am. J. Obstet. Gynecol.* **175**, 853–858. (doi:10.1016/S0002-9378(96)80012-3)

57. Kilarski WM, Semik D, Roomans GM, Ulmstem U, Severs NJ. 1998 Immunohistochemical analysis of connexins 26, 32 and 43 in rat uterus during late pregnancy: lack of connexin 26 in the myometrium. *Histochem. J.* **30**, 307–316. (doi:10.1023/A:1003224225975)